Multiple Energy Scales at a Quantum Critical Point

P. Gegenwart,[1]*† T. Westerkamp,[1] C. Krellner,[1] Y. Tokiwa,[1]‡ S. Paschen,[1]§
C. Geibel,[1] F. Steglich,[1] E. Abrahams,[2] Q. Si[3]*

We report thermodynamic measurements in a magnetic-field-driven quantum critical point of a heavy fermion metal, YbRh$_2$Si$_2$. The data provide evidence for an energy scale in the equilibrium excitation spectrum that is in addition to the one expected from the slow fluctuations of the order parameter. Both energy scales approach zero as the quantum critical point is reached, thereby providing evidence for a new class of quantum criticality.

Quantum criticality encodes the strong fluctuations of matter undergoing a second-order phase transition at zero temperature. It underlies the unusual properties observed in a host of quantum materials. A basic question that remains unsettled concerns its proper theoretical description, which is challenging because the fluctuations are both collective and quantum mechanical. One class of theory, based on the traditional formulation of classical critical phenomena (1), considers the fluctuations of a classical variable—Laudau's order parameter—in both spatial and temporal dimensions (2–5). The slowing down of the order-parameter fluctuations accompanies the divergence of a spatial correlation length; at each value of the tuning parameter, the equilibrium many-body spectrum contains a single-excitation energy scale, which vanishes at the quantum critical point (QCP) (6). An unconventional class of theory (7–9), by contrast, is inherently quantum mechanical; it explicitly invokes quantum entanglement effects, which are manifested through vanishing energy scales that are in addition to the one associated with the slowing down of order-parameter fluctuations. The nature of quantum criticality can therefore be experimentally elucidated by determining whether single or multiple energy scales vanish as the QCP is reached.

We consider the heavy-fermion metal YbRh$_2$Si$_2$ (YRS) and show that multiple energy scales vanish as its QCP is approached and, in addition, suggest that critical electronic modes coexist with the slow fluctuations of the magnetic order parameter. A direct way to probe the intrinsic energy scales in the equilibrium spectrum near a QCP is to measure thermodynamic properties. Another approach is to measure the fluctuation spectrum in equilibrium, for example by inelastic neutron scattering experiments. Such equilibrium methods are in contrast to transport experiments, which are influenced by electronic relaxational properties, especially for anisotropic and multiband systems.

As extraction of critical energy scales requires measurements through fine steps of the control parameter, which is nearly impossible for inelastic neutron scattering, we report here measurements of thermodynamic properties of YRS across its magnetic QCP.
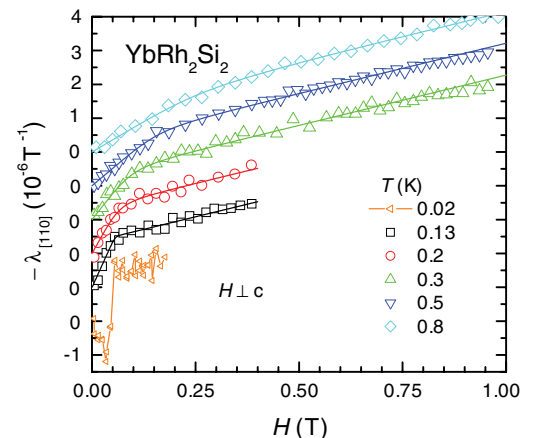
We chose to work with the tetragonal heavy fermion compound YRS because it presents a clean and stoichiometric material that is well characterized (10). In the absence of an external magnetic field, YRS shows very weak antiferromagnetic (AF) order at T_N = 70 mK, with an ordered moment of only ~$10^{-3}\mu_B$/Yb (11). A small magnetic field ($H_{\perp c} \approx 0.06$ T for the field applied within the easy ab plane, and $H_{\|c}$ = 0.66 T along the hard c axis) suppresses the transition temperature and accesses the QCP (12). The ability to use such a small magnetic field to access the QCP makes YRS suited for our purpose; the determination of energy scales requires scanning across the phase transition, and an external magnetic field can be tuned with relative ease and continuously. Hall effect measurements (13) on YRS have shown a large and rapid crossover in the Hall constant at a temperature-dependent magnetic field away from the antiferromagnetic transition. In the zero-temperature limit, this crossover extrapolates to a jump across the QCP, which has been interpreted as a large change of the Fermi surface volume. This represents yet another advantage of measuring the thermodynamic properties in YRS, because they can be compared with their transport counterparts.

We measured the isothermal linear magnetostriction $\partial \ln L / \partial H$, where L is the length along the [110] direction within the tetragonal ab plane, and the magnetic field H is applied along the same direction ($H \perp c$). Figure 1 shows the magnetostriction as a function of the magnetic field, at temperatures ranging from 0.02 K to 0.8 K. For temperatures below 0.075 K, a clear discontinuity is observed when suppressing the AF order by a critical magnetic field. At $T > 0.075$ K, it is seen that, for a small magnetic field, the isothermal magnetostriction linearly depends on the magnetic field, as is the case in typical metals (14). Beyond a crossover field, however, there is a change to a high-field region with a different slope. The crossover field decreases as the temperature is reduced.

To understand this crossover, we compare it with the field-dependent isothermal behavior of other thermodynamic and transport quantities. Figure 2A illustrates the similarity of the crossover in the magnetostriction to that seen in the field-dependent isothermal Hall resistivity ρ_H (measured with $H \| c$). The Hall coefficient was described (13) by an empirical crossover

[1]Max Planck Institute for Chemical Physics of Solids, D-01187 Dresden, Germany. [2]Center for Materials Theory, Department of Physics and Astronomy, Rutgers University, Piscataway, NJ 08855, USA. [3]Department of Physics and Astronomy, Rice University, Houston, TX 77005, USA.

*To whom correspondence should be addressed. E-mail: pgegenw@gwdg.de (P.G.); qmsi@rice.edu (Q.S.)
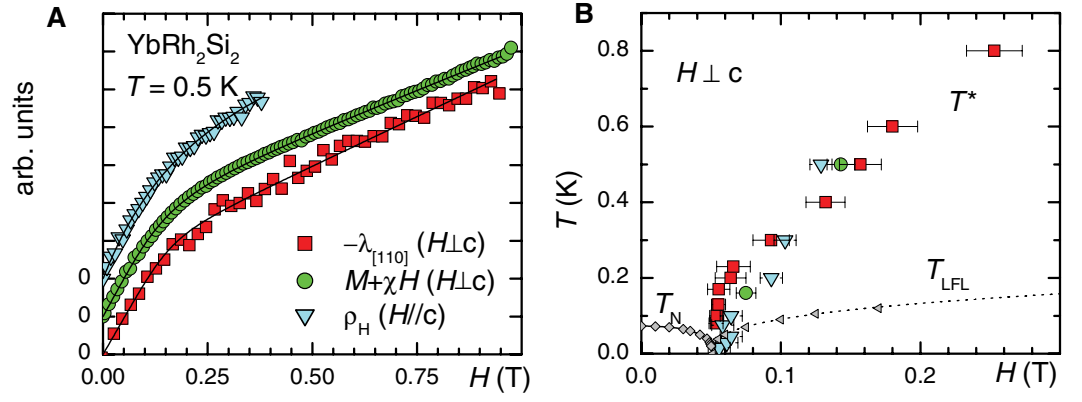†Present address: First Physics Institute, University of Goettingen, 37077 Goettingen, Germany.
‡Present address: Los Alamos National Laboratory, Los Alamos, NM 87545, USA.
§Present address: Institute of Solid State Physics, Vienna University of Technology, 1040 Vienna, Austria.

Fig. 1. Magnetic-field dependence of the magnetostriction of YbRh$_2$Si$_2$. The symbols represent the linear coefficient $\lambda_{[110]} = \partial \ln L / \partial H$ (where L is the sample length along the [110] direction within the tetragonal ab plane) versus H at various temperatures. Note that $\lambda_{[110]} < 0$ and that the data sets have been shifted by different amounts vertically. The sharp feature in the 0.02 K data corresponds to a discontinuity in λ (as is more clearly seen in the measured length versus H, which shows a change in slope but does not contain any discontinuity), demonstrating the continuous nature of the magnetic transition at the critical field of 0.05 T. Similar behavior is observed at various different temperatures below 0.075 K, for example, at 0.03 K and 0.05 K. The solid lines for $T \geq 0.13$ K are fits using the integral of the crossover function $f(H,T)$, which reveal a characteristic field scale $H_0(T)$ along which the magnetostriction shows a drastic change in slope.

Fig. 2. Energy scales in $YbRh_2Si_2$, determined from thermodynamic, magnetic, and transport measurements. (**A**) The field dependence ($H \perp c$) of the magnetostriction $\lambda_{[110]}$, $\tilde{M} \equiv M + \chi H$ (where $\chi = \partial M/\partial H$), and the Hall resistivity ρ_H for $H \| c$ (for the latter, the field values have been divided by the anisotropy factor 13.2, which corresponds to the ratio of the critical fields in the Hall and magnetostriction measurements), respectively, all at $T = 0.5$ K; similar behavior is observed at other temperatures. For $\lambda_{[110]}(H \perp c)$, the sample has a residual resistivity $\rho_0 =$

0.5 $\mu\Omega$ cm and $H_c = 0.05$ T; for $\tilde{M}$ ($H \perp c$), the sample has $\rho_0 = 1.0$ $\mu\Omega$ cm and $H_c = 0.06$ T; and for $\rho_H(H \| c)$, the sample has $\rho_0 = 1.0$ $\mu\Omega$ cm and $H_c = 0.66$ T. The solid lines correspond to fits using the integral of the same crossover function $f(H,T)$. Each data set has been normalized by its initial slope. For clarity, the three data sets have been shifted by different amounts vertically: This is represented by the three separate zero marks along the vertical axis for the three quantities. $\rho_H - \rho_{H,a}$, where $\rho_{H,a}$ is the anomalous Hall resistivity (13), behaves similarly to ρ_H. We analyzed $\tilde{M}(H)$, which is the field derivative of the magnetic free energy contribution ($-M \times H$); fitting $M(H)$ leads to similar conclusions, although the quality of the fit is somewhat poorer because M versus H is not as

linear as $\tilde{M}$ at high fields (fig. S2). (**B**) The crossover field scale H_0 as determined from magnetostriction, $\tilde{M}$, and Hall resistivity using the same symbols as in A. It is equivalent to the energy scale $T^*(H)$. The gray diamonds and triangles represent, respectively, the Néel ordering temperature (T_N) and the crossover temperature (T_{LFL}), below which the electrical resistivity has the Fermi liquid form $\rho = \rho_0 + AT^2$, as determined from measurements on a single crystal with $\rho_0 = 0.5$ $\mu\Omega$ cm and $H_c = 0.05$ T. The solid and dotted lines are guides to the eye; for the latter, data points outside the plotted field regime have also been used. The horizontal error bars represent the fitting error rather than the width of the crossover.

function of the form $f(H,T) = A_2 - (A_2 - A_1)/[1 + (H/H_0)^p]$; the crossover field scale $H_0(T)$ is equivalent to an energy scale $T^*(H)$. We have analyzed the magnetostriction data, as well as the existing magnetization data ($H \perp c$) (15, 16), with the same crossover function. No corresponding anomalies can be resolved in the magnetization data for $H \| c$ (16), which is almost linear in H. The solid curves in Fig. 1 and Fig. 2A correspond to fits of $\lambda_{[110]}$, $\tilde{M} \equiv M + \chi H$ and the Hall resistivity ρ_H. Figure 2B shows the three sets of $H_0(T)$ obtained from such fits. Their overlap represents a key conclusion of the present work; it suggests that they define one energy scale $T^*(H)$. This scale is seen to be distinct from either the transition temperature (T_N) for the magnetic ordering at $H < H_c$ or the scale (T_{LFL}) for the establishment of the Landau Fermi liquid state at $H > H_c$. For all three quantities, the width of the crossover extrapolates to zero at $T = 0$, implying that the differentials of the magnetostriction, magnetization, and Hall resistivity have a jump in the zero-temperature limit (supporting online text).

The results raise the important question of the causal relation between the thermodynamic and electronic transport properties. One might argue (17) that the Hall-effect evolution as a function of the magnetic field (13) is caused by the Zeeman splitting of the Fermi surface induced by the magnetization (and reflected in the magnetostriction). However, the magnetization only displays a smeared kink, and the corresponding Fermi surface change would at most produce a smeared kink in the evolution of the Hall coefficient; such a kink is too weak compared with the smeared jump seen experimen-

Fig. 3. Longitudinal magnetoresistivity of $YbRh_2Si_2$ as ρ versus H ($H \perp c$) at various temperatures. The maxima in the 0.03 and 0.07 K data indicate the boundary of the AF ordered state [$T_N(H = 0) = 0.075$ K]. The arrows mark the positions of inflection points in $\rho(H)$. The inset A displays the phase diagram, where the gray shaded area represents the range of $H_0(T)$ values shown in Fig. 2B. Open yellow triangles mark the positions of the inflection points in the longitudinal electrical resistivity. The smeared kink behavior in the isothermal M versus H corresponds to a peak in the T

dependence of χ. The latter has been observed (20); the corresponding peak temperature versus H for a sample with $\rho_0 = 0.5$ $\mu\Omega$ cm and $H_c = 0.05$ T is displayed by the dark blue diamonds and found to be consistent with $H_0(T)$. Inset B displays the derivative $d\rho/dH$ versus H at both $T = 0.1$ K and $T = 0.3$ K. Arrows mark the minima, corresponding to the inflection points in $\rho(H)$.
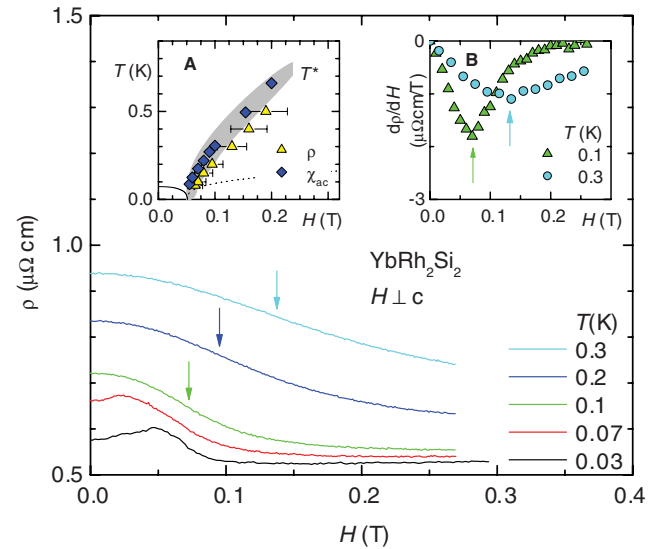
tally. Moreover, along the c axis, even such a smeared kink feature is absent in the magnetization versus the magnetic field. Instead, it is more natural to view the nonanalyticities in both the magnetostriction and magnetization as thermodynamic manifestations of the large Fermi surface jump caused by an f-electron localization.

To explore this issue further, we have also studied the longitudinal magnetoresistivity. Figure 3 shows the electrical resistivity ρ as a function of the magnetic field ($H \perp c$), at various

temperatures. The broadened steplike decrease, observed at all temperatures, corresponds to the crossover observed in the other properties. Indeed, as shown in inset A, the crossover fields determined from the minima of the derivative $d\rho/dH$ (inset B) fall on the same $T^*(H)$ line determined from the magnetostriction, magnetization, and Hall effect. In addition, inset B shows that the width of the crossover decreases as the temperature is lowered. A detailed analysis shows that the crossover width goes to zero in the zero-temperature
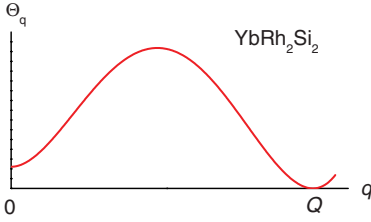
Fig. 4. Sketch of the suggested **q** dependence of the Weiss temperature $\Theta_{\mathbf{q}}$, which enters the magnetic susceptibility. As H reaches H_c, it vanishes at the antiferromagnetic wave vector **Q**, as shown. In addition, $\Theta_{\mathbf{q}}$ has a second minimum at **q** = 0. Ferromagnetic fluctuations at **q** = 0 remain important as $\Theta_{\mathbf{q} = \mathbf{Q}}$ goes to zero.

limit (supporting online text), implying a jump in the residual resistivity across the magnetic QCP. This is in accordance with the theoretical expectations (*18, 19*) associated with an *f*-electron localization transition.

Figure 3, inset A, also shows the temperature scale as a function of field, extracted from the peak in the *T*-dependence of the differential susceptibility $\chi_{ac} = \partial M/\partial H$; the latter, observed earlier (*20*), necessarily accompanies the smeared kink behavior in the isothermal *M* versus *H*. It is clearly seen that this scale too falls on the same *T**(*H*) line.

Our results shed light on the overall phase diagram of this clean stoichiometric quantum critical material. Nuclear magnetic resonance (NMR) measurements (*21*), while signaling the dominance of AF fluctuations in the quantum critical regime, have also revealed enhanced ferromagnetic fluctuations. The Korringa ratio, $S = 1/T_1 TK^2$, is small—on the order of $0.1S_0$, where S_0 is the corresponding ratio for non-interacting electrons. Further evidence for enhanced ferromagnetic fluctuations has come from magnetization measurements (*20*). The Wilson ratio—$R_W = \pi k_B^2/(\mu_0\mu^2_{eff}) \times \chi/\gamma$, with $\mu_{eff} = 1.4\ \mu_B/$Yb (*22*)—is strongly enhanced for an extended region of the phase diagram. It is already large (~20) for magnetic fields of a few teslas and further increases as the field is reduced toward H_c. Therefore, it could be tempting to consider the **q** ~ 0 magnetic fluctuation as the dominant critical fluctuation (*17*), especially because a conventional ferro-magnetic QCP would yield a Grüneisen exponent (*23*) of $1/zv = 2/3$, close to what is observed in YRS (*24*). This picture is problematic for a number of reasons, however. First, neither three-dimensional (3D) nor 2D ferro-magnetic spin fluctuations can generate the fractional exponent observed in the temperature dependence of the uniform spin susceptibility (*20*). Second, ferromagnetic spin fluctuations would lead to a divergent $1/T_1$ (~$1/T^x$, with $x = 1/3$ and $1/2$ for 3D and 2D cases, respectively) that is in contrast to the observation that $1/T_1$ is approximately constant when the NMR measurement field is extrapolated to the quantum

critical regime (*11*). Third, because ferro-magnetic spin fluctuations are inefficient in affecting charge transport, this picture contradicts the observation of a nearly *H*-independent ratio A/χ^2 that accompanies a strongly *H*-dependent *A* and χ (*20*). Here, *A* is the coefficient of the T^2 component of the resistivity.

The data presented here show that the uniform magnetization (**q** = 0) depends on the same underlying physics as that for the charge transport. Because the transport is dominated by large **q** fluctuations, the results imply that the **q** = 0 magnetic fluctuations are a part of overall fluctuations in an extended range of wave-vector scales. It is then more natural to assume that the dynamical spin susceptibility at different wave vectors obeys the same form (*8, 25*) as that observed in another prototypical quantum critical heavy fermion metal, CeCu$_{5.9}$Au$_{0.1}$ (*17*): $\chi(\mathbf{q},T,\Omega) \sim [\Theta_{\mathbf{q}} + T^\alpha W(\omega/T)]^{-1}$. At the QCP, the Weiss field at the antiferromagnetic wave vector (**q** = **Q**) vanishes: $\Theta_{\mathbf{Q}} = 0$. At the same time, and unlike for CeCu$_{5.9}$Au$_{0.1}$, $\Theta_{\mathbf{q}=0}$ is very small in YRS. Based on the saturation scale seen in the temperature dependence of the uniform magnetic susceptibility (*20*) and the NMR Knight shift data (*21*) near H_c, we estimate $\Theta_{\mathbf{q} = 0}$ to be on the order of 0.3 K (*26*). When **q** moves away from either 0 or **Q**, $\Theta_{\mathbf{q}}$ increases to the order of the Ruderman-Kittel-Kasuya-Yosida (RKKY) interaction or bare Kondo scale [about 25 K for YRS (*10*)], as illustrated in Fig. 4. The enhanced uniform magnetic susceptibility, the concomitant enhanced Wilson ratio (*20*), and the small $S \equiv 1/T_1 TK^2$ naturally follow from this picture. Moreover, both $\chi_{\mathbf{q}=0}$ and $\chi_{\mathbf{q}=\mathbf{Q}}$ scale similarly with *H*, and the observation that A/χ^2 is nearly *H*-independent is in fact a manifestation of an *H*-independent $A/\chi^2_{\mathbf{Q}}$. All this leads to the conclusion that the origin of the *T** line lies in an electronic slowing down and, for YRS, the strong **q** = 0 fluctuations happen to be a consequence of the latter as well.

We now turn to more detailed theoretical implications of our results. Our measurements establish that the energy scale *T** is associated with the equilibrium many-body spectrum (which alone determines thermodynamics). Moreover, this scale is distinct from the Landau Fermi liquid scale, T_{LFL}, because physical quantities manifest rather different behavior across the two scales (supporting online text). Finally, both of these scales vanish at the QCP. These findings contradict the conventional order-parameter fluctuation theory in at least two respects. First, the only low-energy scale in that theory is associated with the magnetic slowing down which, for $H > H_c$, is T_{LFL} (*2–5*). Second, within that theory, a sharp feature in thermodynamics and transport quantities might arise near T_N only.

Our results are instead consistent with magnetic quantum criticality accompanied by the

destruction of Kondo entanglement. In the form of local quantum criticality (*7, 8*), a collapse of a large Fermi surface as *H* decreases leads to an added energy scale characterizing an electronic slowing down and, in addition, yields a zero-temperature jump in the Hall coefficient and in the field differentials of the thermodynamic quantities. An additional vanishing energy scale also exists in the "deconfined" quantum criticality scenario for insulating quantum magnets (*9*), as well as in its extension to itinerant electron systems (*27, 28*) that are argued to be relevant to quantum critical heavy fermion metals.

References and Notes
1. K. G. Wilson, *Rev. Mod. Phys.* **55**, 583 (1983).
2. J. A. Hertz, *Phys. Rev. B* **14**, 1165 (1976).
3. A. J. Millis, *Phys. Rev. B* **48**, 7183 (1993).
4. T. Moriya, T. Takimoto, *J. Phys. Soc. Jpn.* **64**, 960 (1995).
5. N. D. Mathur *et al.*, *Nature* **394**, 39 (1998).
6. S. Sachdev, *Quantum Phase Transitions* (Cambridge Univ. Press, Cambridge, 1999).
7. P. Coleman, C. Pépin, Q. Si, R. Ramazashvili, *J. Phys. Cond. Matt.* **13**, R723 (2001).
8. Q. Si, S. Rabello, K. Ingersent, J. L. Smith, *Nature* **413**, 804 (2001).
9. T. Senthil, A. Vishwanath, L. Balents, S. Sachdev, M. P. A. Fisher, *Science* **303**, 1490 (2004).
10. O. Trovarelli *et al.*, *Phys. Rev. Lett.* **85**, 626 (2000).
11. K. Ishida *et al.*, *Phys. Rev. B* **68**, 184401 (2003).
12. P. Gegenwart *et al.*, *Phys. Rev. Lett.* **89**, 056402 (2002).
13. S. Paschen *et al.*, *Nature* **432**, 881 (2004).
14. B. S. Chandrasekhar, E. Fawcett, *Adv. Phys.* **20**, 775 (1971).
15. Y. Tokiwa *et al.*, *Phys. Rev. Lett.* **94**, 226402 (2005).
16. P. Gegenwart, Y. Tokiwa, J. Custers, C. Geibel, F. Steglich, *J. Phys. Soc. Jpn.* **75** (suppl.), 155 (2006).
17. H. v. Löhneysen, A. Rosch, M. Vojta, P. Wölfle, http://arxiv.org/abs/cond-mat/0606317 (2006).
18. P. Coleman, J. B. Marston, A. J. Schofield, *Phys. Rev. B* **72**, 245111 (2005).
19. Q. Si, S. Rabello, K. Ingersent, J. L. Smith, *Phys. Rev. B* **68**, 115103 (2003).
20. P. Gegenwart, J. Custers, Y. Tokiwa, C. Geibel, F. Steglich, *Phys. Rev. Lett.* **94**, 076402 (2005).
21. K. Ishida *et al.*, *Phys. Rev. Lett.* **89**, 107202 (2002).
22. J. Custers *et al.*, *Nature* **424**, 524 (2003).
23. L. Zhu, M. Garst, A. Rosch, Q. Si, *Phys. Rev. Lett.* **91**, 066404 (2003).
24. R. Küchler *et al.*, *Phys. Rev. Lett.* **91**, 066405 (2003).
25. A. Schröder *et al.*, *Nature* **407**, 351 (2000).
26. More specifically, the data over the temperature range of 0.3 K < *T* < 10 K are fitted with $\alpha = 0.6$ and $\Theta_{\mathbf{q}=0} \approx 0$, whereas those for *T* < 0.3 K by $\alpha = 1$ and $\Theta_{\mathbf{q}=0} = 0.3$ K (*22*).
27. T. Senthil, M. Vojta, S. Sachdev, *Phys. Rev. B* **69**, 035111 (2004).
28. T. Senthil, S. Sachdev, M. Vojta, *Physica B* **359-361**, 9 (2005).
29. We would like to thank P. Coleman, J. Custers, Z. Fisk, S. Friedemann, K. Ishida, S. Kirchner, D. Natelson, N. Oeschler, and S. Wirth for useful discussions. This work has been supported by the Fonds der Chemischen Industrie, NSF grant DMR-0424125, and the Robert A. Welch Foundation.